


Structural, morphological, optical, magnetic and ferroelectric properties of $\text{Ba}_{0.2}\text{La}_{0.8}\text{Fe}_2\text{O}_4$ nanofibers

U. Naresh¹, Rapole Jeevan Kumar¹, Kadiyala Chandra Babu Naidu^{2,*} 

¹Department of Physics, Sri Krishnadevaraya University, Ananthapuram-515003, A.P, India

²Dept. of Physics, GITAM Deemed to be University, Bangalore-562163, Karnataka, India

*corresponding author e-mail address: chandrababu954@gmail.com | Scopus ID: [56520309700](https://orcid.org/56520309700)

ABSTRACT

The structural, morphological, optical, magnetic, and ferroelectric properties were studied for the $\text{Ba}_{0.2}\text{La}_{0.8}\text{Fe}_2\text{O}_4$ (BLF) through hydrothermal method. The face-centered cubic structure is confirmed from the X-Ray diffraction (XRD) analysis with some impurities. The particle size calculated from XRD is 21 nm. The Fourier transform infrared spectroscopy (FTIR) revealed the spinel structure of the synthesized samples. The surface morphology analyzed with the help of field emission scanning electron microscopy, transmission electron microscope. In addition, UV-Visible spectroscopy was used for the energy band gap (E_g) estimation and it is found as 2.05 eV. The M-H loop analysis makes clear that the synthesized samples have low magnetization with a small loop area. The P-E loop analysis expressed the ferroelectric nature of the synthesized sample.

Keywords: Structure; Nanoparticles; Band-gap; Magnetic properties.

1. INTRODUCTION

It was well known fact that the magnetic materials are one of the most used materials for information storage devices such as hard disk, floppy disk electronic chip etc. However, the technology needs the reduction of size and increment of storage capacity, better mechanical strength to facilitate the memory storage applications [1]. Furthermore, the low energy gap and well optical properties with magnetic nature can be used in magneto ceramics, magnetocaloric effect application for the multipurpose. Also, various engineering and electronic application like an electronic chip, memory storage devices, high energy power transformer core, shielding of electromagnetic waves, on the other hand, biomedical application such as drug delivery, MRI imaging technology, hyperthermia cancer treatment [2] etc.

Generally, the ferrites are part of the magnetic materials. However, Magnetic materials divided as dia (Ba, La, Cu...etc), para (O, Mg, Na...etc), and Ferro (Ni, Co, Fe...etc) magnetic materials based on the susceptibility increment not only this three types but also have another type of materials like ferrites (AB_2O_4), granites $\text{AB}_{12}\text{O}_{16}$ are the commonly used for the industrial applications. In particular, ferrites are divided into two types such as soft ferrites (small loop area) which are more suitable for medical applications and hard ferrite (broad loop area) which is used for the transformer cores, permanent storage devices. In present concerns, the soft ferrite magnetic materials having spinel structure with specified formula AB_2O_4 where A refers the divalent cations like Co, Cu, Mg, Zn, Mn, Ni, etc., and B relates to the trivalent iron atoms [3].

In the group of ferrites, the barium ferrites accomplish an interest due to ferroelectric nature and magneto ceramic characteristics and having ceramic pigment properties [4]. The rare earth elements have larger radii hence the rare earth integrated into ferrites happens lattice imperfections [5]. In general

magnetization, optical band gap, and ferroelectric properties altered by the Fe-Fe interactions and Fe- rare earth elements. All of the rare earth series lanthanum (La^{+3}) is the specialized candidate to alter the physical properties of the material due to the greater ionic radius which is nearly (1.22 Å), in addition, La^{+3} is diamagnetic (non-magnetic) cations [6]. Even so, replacement of larger ionic radii in place of Ba and Fe radii can change structural and magnetic properties by attributing lattice strain in the material. Whereas the exchange interaction between tetrahedral and octahedral site might not be taken responsibly in this case to increase magnetization of the ferrite system, finally the magnetization of nonmagnetic rare earth element could not effect because of exchange of cations but it can change structural properties to engage magnetic properties ferrite systems [7]. Hence, incorporation of greater ionic radii induces lattice strain it causes an increase of the particle size; therefore the size of material could be achieved as required industrial application. The incorporation of La^{3+} ions into $\text{Ba}_{0.2}\text{Fe}_2\text{O}_4$ system represents changes in physicochemical properties. The literature revealed the influence of La ($x = 0.8$) on structural and morphological, magnetic, optical, Ferro-electric properties of $\text{Ba}_{0.2}\text{Fe}_2\text{O}_4$ not reported in available literature. The variation of rare-earth ions replaces the generation of oxygen spaces for reimbursement charges. Larger molecular radius La^{3+} (1.22 Å) compared with Fe^{+3} (0.64 Å), affects magnetization by breaking spin cycloid in the barium ferrite system. Therefore, the authors interested in synthesizing and to study the properties like structural, optical, morphological, magnetic and ferroelectric properties of La-doped Ba ferrite nanoparticles.

Further, the preparation of nanomaterials is a key factor to facilitate the physical properties of the materials. More generally, usual synthesis methods are like sol-gel method, solvothermal

method, hydrothermal technique, chemical co-precipitation, microemulsion, polyol method, and auto-combustion technique [8]. The hydrothermal method is the accurate and feasible method to synthesize nanoparticles owing to single phase production, control of size.

Moreover, some of the previous reports exercised with this type of materials very interestingly in many areas viewing to their multi ferric nature and narrow optical band gap. Qing Lin et al [9]. Synthesized Mg, Ba dual doped $\text{La}_{0.85}\text{FeO}_3$ particles in nanometer size via sol-gel method it was found that the particle size depends upon the preparation method, whereas they found that low-temperature calcination is probably good for getting pure phase in XRD, on the other hand, the VSM studies show the Ba^{+2} can increase the H_c value. In a similar way, the ferrite-based composites such as polyaniline, polypyrrole mixed with ferrites

could be permitted for the fabrication of multi-efficient materials for electronic devices and sensors applications [4-5].

$\text{La}_{0.8}$ substituted $\text{Ba}_{0.2}\text{Fe}_2\text{O}_4$ for structural, optical, magnetic, and ferroelectric properties through the hydrothermal method followed by predictable heating at 573 K was done in this work. Indeed, the hydrothermal method followed by low temperature can provide a single phase having well morphology. It can be estimated that La substituted barium ferrite shows the reduction in magnetization (M_s) as well as enhancement in the energy band gap. These types of systems may be well suited for biomedical application such as hyperthermia treatment and drug delivery systems. Moreover, there were limited works done so far on the La incorporated barium ferrite nanoparticles via the hydrothermal route.

2. MATERIALS AND METHODS

The chemicals of La $(\text{NO}_3)_2 \cdot 6\text{H}_2\text{O}$, Ba $(\text{NO}_3)_2 \cdot 6\text{H}_2\text{O}$, Fe $(\text{NO}_3)_3 \cdot 9\text{H}_2\text{O}$ & NaOH (Sigma- Aldrich) were selected as the precursors. La $(\text{NO}_3)_2 \cdot 6\text{H}_2\text{O}$, Fe $(\text{NO}_3)_3 \cdot 9\text{H}_2\text{O}$ & Ba $(\text{NO}_3)_2 \cdot 6\text{H}_2\text{O}$, Fe $(\text{NO}_3)_3 \cdot 9\text{H}_2\text{O}$ mixed in a laboratory glass beaker using magnetic stirrer in distilled water (1:4) Nitrates: water separately as per the planned stoichiometric calculation. The stirring process continued at constant pH values (pH = 11) through the addition of the NaOH slowly to the mixer. After, the reacted homogeneously mixed brown colored solution was transferred into 300 ml autoclave (steel lined Teflon jar). The sealed autoclave was fetched into a hot air oven. The temperature of the oven kept at 150°C and time setup is 8 hrs. Further, the reacted solution was

washed with the acetone and distills water several times till it got purified, then this purified content dried at 100°C in the oven for two hours. Finally, fine powder type samples were collected. These samples are characterized to study structural, morphological, optical, magnetic properties using X-ray diffraction, Fourier transforms infrared spectroscopy (FTIR), Field emission scanning electron microscopy, and Transmission electron on microscopy (FESEM, TEM), Energy Dispersive X-ray analyzer (EDAX), UV- Visible spectroscopy, vibrating sample magnetometer (VSM) respectively, and P-E loop tracer used to detect ferroelectric nature.

3. RESULTS

3.1. X-Ray Diffraction (XRD) Analysis.

Figure.1 illustrates the revealed patterns of X-ray diffraction for the synthesized material of $\text{Ba}_{0.2}\text{La}_{0.8}\text{Fe}_2\text{O}_4$. The XRD outline could be evidenced that the synthesized nanoparticles showing the developed cubic spinel phase formation including some impurity phases. These are found at two-theta angles around 40.812 , 32.186 , 50.614 , 54.409 , 64.814 and 71.883° . They are associated to the perovskite phases of BaFeO_3 and LaFeO_3 . In general, this is happened owing to the incorporation of trivalent ion into the divalent element. Similar observation is noticed in reference [6].

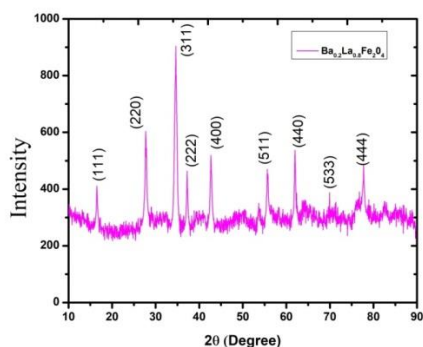


Figure 1. X-ray diffraction spectra of the BLF nanoparticles.

This confirmed a fact that the formed cubic spinel phases are not pure. However, we considered them as the maximum intense

peaks for evaluating the structural parameters of cubic spinel structure. These reflection planes of (111), (220), (311), (222), (400), (511), (440), (533), (444) are in relation with the cubic spinel phases of JCPDS: 25-0283 pattern. The crystallite size (D) was calculated using the average crystallite $D = 0.9\lambda/\beta\cos\theta$, where λ = wavelength of X- rays and β is full width half maximum [10-11] for the maximum reflection plane or cubic characteristic plane (311) it was found as 21 nm. Also, micro-strain (ϵ) was premeditated using principle $\epsilon = \beta/4\tan\theta$ and the results were accounted in Table.1 [12].

On the other hand, the lattice parameter was found using the familiar formula $a = d(h^2 + k^2 + l^2)^{1/2}$ for the same reflection plane (311) and that value is 9.85 nm. The radii of synthesized elements can be affected in the octahedral tetrahedral occupation Ba^{+2} : 1.35 Å, La^{+3} : 1.22 Å, Fe^{+3} : 0.645 Å [13]. The difference between Ba^{+2} and La^{+3} radii makes strain in lattice structure which is due to the distribution of cations of different ionic radii between the tetrahedral site and octahedral site. The incorporation of La^{+3} atoms replaces Fe^{+2} atoms owing to the greater ionic radii of La^{+3} than the Fe^{+2} radii. This leads to a larger value of lattice parameter which could become a reason for the larger volume which is found as 955.67 \AA^3 . In addition, the theoretical density was calculated by using the statement $\rho_t = 8M/\text{Na}^3$ (where 'M' is molecular weight, 'N' is Avogadro's number, and 'a' is lattice constant) it

was presented in Table.1. Later, the BLF nano particle's bulk density samples assessed using the formulation $\rho_e = m/\pi r^2 t$, here m is mass, r is radius, and t is the thickness of pellets. Afterward, porosity: $P = 1 - (\rho_e/\rho_t)$ [2] is calculated for the synthesized sample (Table.1). The specific surface area of the sample was established with the help of relation [2]: $S = 6000/(D*\rho_e)$, where D , and ρ_e have their usual meaning.

3.2. Morphological Properties.

The surface analysis of the barium lanthanum ferrite (BLF) nanoparticle was studied with the help of Field emission scanning electron microscopy, and Transmission electron microscopy. The FESEM image (Fig.3) reflects morphological aspects such as the shape of the nanoparticles as well as distribution grains. Hence, in the micrographs, the grain size of the particle was found using the linear intercept method: $G_a = 3d/2MN$, here 'd' pass on to the testing line distance, 'M' is connected to the magnification used and 'N' is coupled to the number of grains touching to the testing line [6].

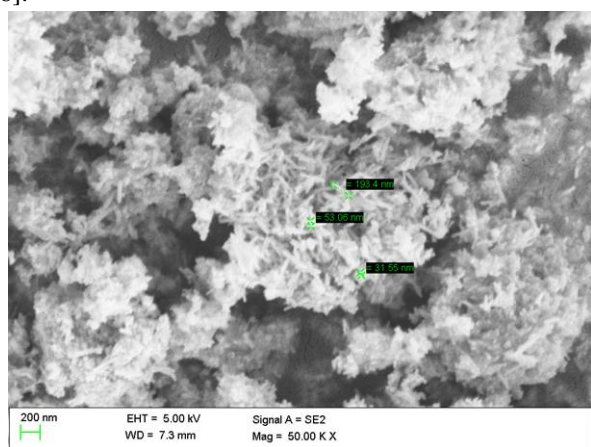


Figure 3.FESEM image of the BLF nanoparticles.

The 24.7 nm sized particles and the partial agglomeration between the particles observed. However, The EDAX spectra of synthesized nanoparticles show no impurities involved in the material as appears in Fig.4. On the other hand, The appearance of the TEM images shows synthesized particles oriented as nanofibers with the size 20 nm - 100 nm as shown in Fig.5, it was noticed that the group of nanofiber grains was distributed equivalently, Moreover, the growth of nano fibers with a group is

due to the magnetic interactions between the nanoparticles. This fiber grains was occurred due to the presence of rare earth element (La) this type of fiber formation by incorporating La⁺³ was reported in previous paper. The hydrothermal treatment supported the formation of nanofibers. This type of confirmation was reported in the literature [3]. This kind of nanofiber formation and its clusters are well suited in the drug delivery and related biomedical functions [3].

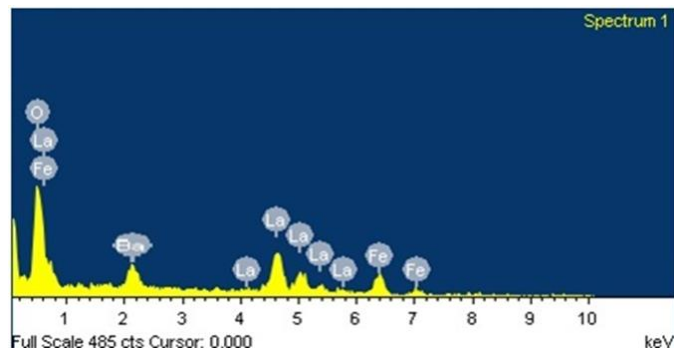


Figure 4.EDS spectra of the BLF nanoparticles.

Actually, the huge number of ferroelectric domains of Ba, La elements may induce the elongated fibers. Suresh et al. reported the lanthanum doped cobalt titanate nanoparticles; they found lanthanum incorporation supports to the fiber formation also which are elongated by ferroelectric cations. In addition, the size of the particles observed between 10 nm - 70nm. The morphology of synthesized particles agreed on the fact which is the grain size greater than the particles size it could be happened by agglomeration [3].

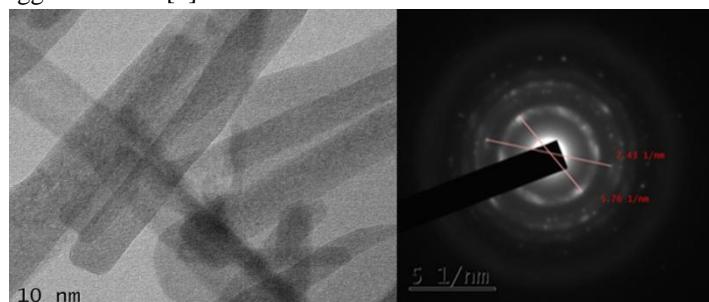


Figure 5.TEM picture and SAED of BLF samples.

Table 1. Structural properties of the BLF nanoparticles.

x	a (Å)	FWHM	D (nm)	V(Å) ³	ρ_t (g/cm ³)	ρ_e (g/cm ³)	porosity (P)	ϵ	S (m ² /g)	G _a (nm)	v_1 (cm ⁻¹)	v_2 (cm ⁻¹)
BLF	9.85	0.02481	21	955.67	3.74	2.69	0.28	0.00281	57	24.257	569.21	418

3.3. FT-IR spectral analysis.

The obtained FTIR spectra as shown in Fig.6 represent the formation of the spinel structure of the synthesized samples. The spectra illustrate the two spinel characteristic absorption bonds such as the octahedral bond at 428 cm⁻¹ whereas tetrahedral stretching vibration bond at 569.2 cm⁻¹. Hence, this two bond assignment revealed the arrangement of spinel bonds in the lattice and it was indicated as v_2 , and v_1 , in the Fig.6. Moreover, the additional absorption bonds were observed in the spectra and it was due to iron ions vibrations, and oxygen atoms of the H₂O

molecule [12]. This may be happened due to the strain and crystalline effects.

3.4. UV-Visible spectra.

The UV- Visible spectroscopy is one of the accurate tools for the estimate the energy gap (E_g). Hence, the diffuse reflectance spectra and absorption spectra were carried out and it was represented in the Fig.7. The Energy band gap estimation was carried out using the relation $(\alpha h\nu)^m = k (h\nu - E_g)$ [13] where 'h ν ' is the energy, 'k' is continuous, ' E_g ' is the optical band-gap and' is expressed as the type of transition. The $\alpha h\nu$ is measured in eV/cm. In the present work the 'm' value taken as 2 because the transition

is direct. In Fig.7 extrapolated linear portion shows the optical band gap value. The E_g value was found as 2.05 eV it indicates the proper value of the absorption value as shown in Fig.7. These E_g values are little in scale. Therefore, the BLF nanofibers can articulate in optoelectronic devices, photocatalytic and sensor-based purpose [12-13].

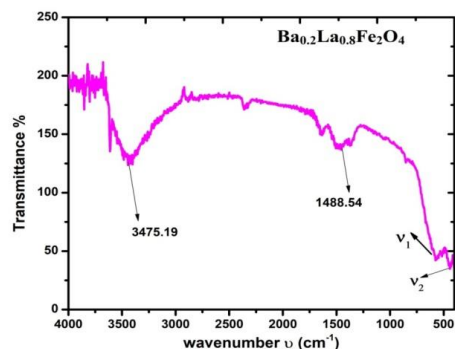


Figure 6. FTIR band spectrum of the BLF nanoparticle.

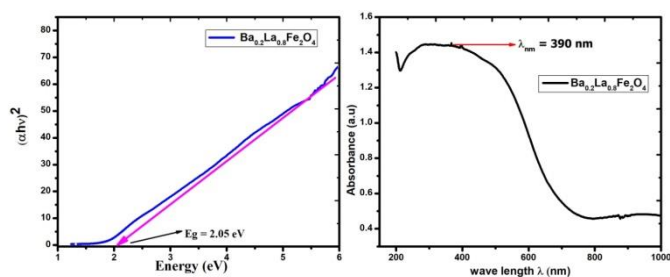


Figure 7. Optical band-gap determination of BLF nanomaterials.

3.5. Magnetic Properties.

M-H loop studies (Fig.8) or hysteresis loop obtained from the vibrating sample magnetometer. The saturation magnetization, coercivity and retentivity evaluated using vibrating sample magnetometer at room temperature. it was noticed the hysteresis curve shows diamagnetic nature and low saturation magnetization (M_s) it is 0.24 G, coercivity (H_c) 0.04 G, remanence magnetization (M_r) 0.06 emu^{-1} . The saturation magnetization of the synthesized sample obtained at 0.3. These properties show the synthesized sample has nonmagnetic nature. The reason for the nonmagnetic nature revealed may be increasing non-magnetic cations in B site that is octahedral site. The distribution of cations was probably

4. CONCLUSIONS

$\text{Ba}_{0.2}\text{La}_{0.8}\text{Fe}_2\text{O}_4$ (BLF) nanoparticles were synthesized via a low-temperature hydrothermal process. The structural properties such as particle size, porosity, and the lattice constant were evaluated from the X-ray diffraction. The morphology was studied by using the FESEM and TEM the studies express the well-formed grains and particles size in nano level of the synthesized. Moreover, the energy band gap was calculated from the UV-

5. REFERENCES

1. Vinuthna, C.H.; Chandra, K.B.N.; Sekhar, C.C.; Ravinder, D. Magnetic and Antimicrobial Properties of Cobalt Zinc Ferrite Nanoparticles Synthesized By Citrate-Gel Method. *International*

estimated based on the well-known theory Two-sub lattice model. The La^{+3} cations replaced the magnetic cations in the B site which is the source of magnetization. Hence, the exchange of nonmagnetic cations La^{+3} in the place of Fe^{+3} can make the decrease of the magnetization [14 - 16].

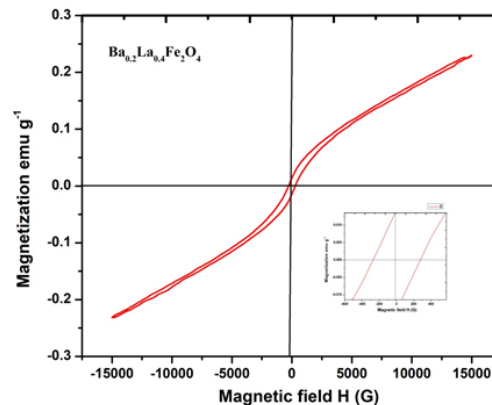


Figure 8. M-H loop of the BLF nanoparticles.

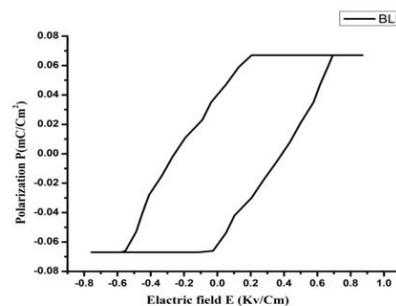


Figure 9. Ferroelectric studies of the BLF particles.

3.6 Ferroelectric Studies.

Fig.9 shows the P-E hysteresis curve of the lanthanum doped barium ferrite nanoparticles (BLF) at 27°C that is room temperature. The ferroelectric parameters found as remanent polarization (P_r) 0.06 mC/cm^2 , saturation polarization (P_s) is 0.075 mC/cm^2 . Herein, the P-E loops of BLF particles are saturated. This may be attributed by low leakage current at the grain boundaries. The grain boundaries block the movement of charges developed due to applied alternating electric field resulting in low values of remanent and saturation polarization of BLF particles. The BLF particles show ferroelectric nature with saturation polarization [17-21].

Visible spectroscopy it was noticed that the sample has the small value of E_g value 2.05 eV is suitable for the optoelectronic application. Finally, the synthesized samples magnetic properties were studied with the help of VSM the M-H curve analysis showed samples very low magnetization indicate the BLF nanoparticle is a diamagnetic material. The ferroelectric properties reflect ferroelectric nature of the material.

Journal of Applied Ceramic Technology 2019, <https://doi.org/10.1111/ijac.13276>.
2. Boda, N.; Boda, G.; Naidu, K.C.B.; Srinivas, M.; Batoo, K.M.; Ravinder, D.; Reddy, A.P. Effect of Rare Earth

Elements on Low Temperature Magnetic Properties of Ni and Co-Ferrite Nanoparticles. *Journal of Magnetism and Magnetic Materials* **2019**, *473*, 228-235, <https://doi.org/10.1016/j.jmmm.2018.10.023>

3. Naresh,U.; Kumar, R.J.; Naidu, K.C.B. Influence of Rare Earth Element on Nanofiber Formation, Optical and Magnetic Properties of Ba_{0.2}Cu_{0.8-x}La_xFe₂O₄ (x = 0.2 - 0.6) Nanoparticles. *Ceram. Int.* **2019**, *45*, 7515–7523, <https://doi.org/10.1016/j.ceramint.2019.01.044>.

4. Farid, M.T.; Ahmad, I.; Kanwal, M.;Murtaza, G.; Ali, I.;Ashiq, M.N.; Khan, S.A. Magnetic and electric behavior of praseodymium substituted CuPr_yFe_{2-y}O₄ ferrites. *Journal of Magnetism and Magnetic Materials* **2017**, *422*, 337–343, <https://doi.org/10.1016/j.jmmm.2016.09.016>.

5. Kothandan, D.;Kumar,R.J.; Naidu,K.C.B. Barium titanate microspheres by low temperature hydrothermal method: studies on structural, morphological, and optical properties. *Journal of Asian Ceramic Societies* **2018**, *6*, <https://doi.org/10.1080/21870764.2018.1439607>.

6. Naresh,U.; Kumar, R.J.; Kothandan, D.;Naidu, K.C.B. Nanofibers Formation and Superparamagnetic Nature of Ba_xCu_{1-x}Fe₂O₄ (x= 0.2- 0.8) Nanoparticles. *Materialchemistry physics* **2019**, *236*, 121807, <https://doi.org/10.1016/j.matchemphys.2019.121807>.

7. Shannon,R.D. Revised Effective Ionic Radii and Systematic Studies of Interatomic Distances in Halides and Chalcogenides. *Acta Cryst. A* **1976**, *32*, 751-767, <https://doi.org/10.1107/S0567739476001551>.

8. Kumar,N.S.; Suvarna,R.P.; Naidu,K.C.B.; Kumar, G.R.;Ramesh,S. Structural and functional properties of sol-gel synthesized and microwave heated Pb_{0.8}Co_{0.2-z}La_zTiO₃ (z = 0.05–0.2) nanoparticles. *Ceramics International* **2018**, *44*, 19408–19420, <https://doi.org/10.1016/j.ceramint.2018.07.176>.

9. Lin, Q.; Lin, J.; Yang, X.; He, Y.; Wang, L.; Dong, J. The effects of Mg²⁺ and Ba²⁺ dopants on the microstructure and magnetic properties of doubly-doped LaFeO₃ perovskite catalytic nano crystals. *Ceramics International* **2019**, *5*, 3333-3340, <https://doi.org/10.1016/j.ceramint.2018.10.246>.

10. Ramaprasad, T.; Kumar,R.J.;Naresh,U.;Prakash,M.;Kothandan,D.; Naidu, K.C. B. Effect of pH Value on Structural and Magnetic Properties of CuFe₂O₄ Nanoparticles Synthesized by Low-Temperature Hydrothermal Technique. *Materials Research Express* **2018**, *5*, 95025.

11. Sandeep Kohli, Patrick R. McCurdy, Derek C. Johnson, Jaydip Das, Amy L. Prieto, Christopher D. Rithner, Ellen R. Fisher, Template-assisted chemical-vapor-deposited spinel Ferrite nanotubes. *J. Phys. Chem. C* **2010**, *114*, 19557–1956, <https://doi.org/10.1021/jp101099u>.

12. Reddy, V.N.; Sarmash, T.S.; Naidu, K.C.B.;Maddaiah,M.;Subbarao, T. Structural and Optical Properties of BaO-ZnO-TiO₂ Ternary System. *Journal of Ovonic Research* **2016**, *12*, 261-266.

13. Kumar,N.S.; Suvarna,R.P.; Naidu,K.C.B. Sol-Gel Synthesized and Microwave Heated Pb_{0.8-y}La_yCo_{0.2}TiO₃ (y= 0.2–0.8) Nanoparticles: Structural, Morphological and Dielectric Properties. *Ceramics International* **2018**, *44*, 18189-18199, <https://doi.org/10.1016/j.ceramint.2018.07.027>.

14. Hashim, M.; Raghasudha,M.;Shah, J.; Shirsath, S.E.; Ravinder,D.;Kumar, S.; Meena, S.S.; Bhatt, P.;Kumar, A.R.;Kotnala,R.K. High-temperature dielectric studies of indium-substituted NiCuZn nano ferrites. *Journal of Physics and Chemistry of Solids* **2018**, *112*, 29-36, <https://doi.org/10.1016/j.jpcs.2017.08.022>.

15. Manohar,A.;Krishnamoorthy,C.; Naidu, K.C.B. Dielectric, Magnetic hyperthermia and Photocatalytic Properties of ZnFe₂O₄ Nanoparticles Synthesized by Solvothermal Reflux method, *Applied Physics A* **2019**, *125*, 477, <https://doi.org/10.1007/s00339-019-2760-0>.

16. Naidu, K.C.B.; Madhuri, W. Ceramic nanoparticle synthesis at lower temperatures for LTCC and MMIC technology. *IEEE Transactions on Magnetics* **2018**, *54*, 2300808, <https://doi.org/10.1109/TMAG.2018.2855663>.

17. Scott, J.F. Ferroelectrics go bananas. *J. Phys.: Condens. Matter* **2008**, *20*, 21001-2.

18. Zouaria,I.;Sassib,Z.;Seveyratb,L.;Abdelmoulaa,N.;Lebrunb, L.;Khemakhem,H. Structural, dielectric, piezoelectric, ferroelectric and electro-caloric properties of Ba_{1-x}Ca_xTi_{0.975}(Nb_{0.5}Yb_{0.5})_{0.025}O₃ lead-free ceramics. *Ceramics International* **2018**, <https://doi.org/10.1016/j.ceramint.2018.01.242>.

19. Kumar,N.S.; Suvarna,R.P.;Naidu, K.C.B. Microwave Heated Lead Cobalt Titanate Nanoparticles Synthesized by Sol-Gel Technique: Structural, Morphological, Dielectric, Impedance and Ferroelectric Properties. *Materials Science and Engineering B* **2019**, *242*, 23-30, <https://doi.org/10.1016/j.mseb.2019.03.005>.

20. Guo-Long, T.; Li, W. Ferroelectricity and ferromagnetism of M-type lead hexaferrites. *J. Am. Ceram. Soc.* **2015**, *98*, 1812–1817, <https://doi.org/10.1111/jace.13530>.

21. Kumar,N.S.; Suvarna,R.P.; Naidu, K.C.B. Multiferroic Nature of Microwave-Processed and Sol-Gel Synthesized NanoPb_{1-x}Co_xTiO₃ (x = 0.2–0.8) *Ceramics. Crystal Research and Technology* **2018**, *53*, 1800139, <https://doi.org/10.1002/crat.201800139>.

22. Guo-Long, T.; Wang, M. Multiferroic PbFe₁₂O₁₉. *J. Electro. Ceram.* **2011**, *26*, 170–174. <https://doi.org/10.1007/s10832-011-9641-z>.

6. ACKNOWLEDGEMENTS

The authors thankful UGC New Delhi for providing financial support under SAP [NO.F 530/5/DRS-II/2016(SAP I)].



© 2019 by the authors. This article is an open access article distributed under the terms and conditions of the Creative Commons Attribution (CC BY) license (<http://creativecommons.org/licenses/by/4.0/>).